RSC Advances

PAPER

View Article Online
View Journal | View Issue

Cite this: *RSC Adv.*, 2016, **6**, 43436

Pyrolyzed carbon with embedded NiO/Ni nanospheres for applications in microelectrodes†

Cong Yin,[a] Liang He,*[a] Yunfei Wang,[a] Zehua Liu,[a] Guobin Zhang,[a] Kangning Zhao,[a] Chunjuan Tang,[ab] Mengyu Yan,[a] Yulai Han[a] and Liqiang Mai*[a]

Received 15th March 2016
Accepted 22nd April 2016

DOI: 10.1039/c6ra06864b

www.rsc.org/advances

Photoresist, a frequently used material in existing microfabrication processes, can be utilized in carbon micro electro mechanical system (C-MEMS) since the patterned carbon micro/nano structures can be formed by pyrolysis of a patterned photoresist. These pyrolyzed carbon microstructures have been used as functional and structural units in carbon-MEMS. Compositing and integration with high performance nanostructures is one important strategy for carbon microstructures with applications in microdevices. Herein, we report a patterned microelectrode of pyrolyzed carbon with embedded NiO/Ni nanospheres (carbon/NiO/Ni) fabricated by a novel microfabrication process combing optimized photolithography with pyrolysis. The microsupercapacitors with interdigital carbon/NiO/Ni (C/NiO/Ni) microelectrodes show a high capacitance of 2.75 mF cm^{-2}. In this microsupercapacitor, the C/NiO/Ni is utilized as the active electrode material and current collector, which makes the microfabrication facile and compatible with micromachining technologies. In addition, the C/NiO/Ni microelectrode pyrolyzed at 900 °C shows a higher capacitance than that of pyrolyzed carbon microelectrodes. The optimized microfabrication process with effectiveness and repeatability shows great potential for fine micropatterning of carbon and electrochemically active materials on a large scale, especially for the microstructuring of a carbon-based composite.

1. Introduction

A micro electro mechanical system (MEMS) is an advanced system based on micro/nano technologies that includes the design, machining and fabrication of microdevices consisting of various micro/nano structures.[1] The high-yield microfabrication process proposed in pyrolyzed carbon based MEMS (C-MEMS) that are fabricated from polymer precursors or a photoresist has outstanding advantages, such as precise control of the morphologies, great repeatability and high resolution of microfabrication, biocompatibility, chemical inertness, *etc.*[2,3] C-MEMS is a potential candidate for high performance microdevices due to its physical and chemical properties, which is complementary to that of silicon based MEMS. Therefore these pyrolyzed carbon structures and C-MEMS have been widely investigated for applications in three-dimensional microbatteries, on-chip supercapacitors, sensors, field emission displays, *etc.*[2–10] Moreover, these pyrolyzed carbon microelectrodes show great potential for applications in energy storage. Various carbon microelectrodes, even some complicated 3-dimensional carbon microelectrodes have been fabricated by photolithography combined with pyrolysis process.[11–14]

Especially, the pyrolyzed carbon microstructures have been served as structural components in C-MEMS due to their high toughness, little mechanical hysteresis and fabrication process can be compatible with microtechnologies.[15–20] Therefore, the pyrolyzed carbon microstructures have often been used as the functional and structural units in C-MEMS. However, the photoresist-derived carbon traditionally shows high stress and shrinkage resulting from its pyrolysis process. As an elastic material in MEMS, one critical problem is the difficulty in obtaining high toughness and high frequency response with little mechanical hysteresis. So the methods to accommodate the stress resulting from the volume shrinkage during the pyrolysis and reinforce the carbon structures show much potential in solving the critical issue of pyrolyzed carbon applied in MEMS. Among some candidates, compositing and integration with uniformly dispersed nanostructures that have high mechanical strength, is one important strategy for carbon microstructures, which is challenging and attractive for applications of carbon micro/nano structures.[1–3]

As we know, high efficient energy storage and conversion system is becoming an increasing demand in our daily life.[21]

---

[a] *State Key Laboratory of Advanced Technology for Materials Synthesis and Processing, Wuhan University of Technology, Wuhan 430070, People's Republic of China. E-mail: mlq518@whut.edu.cn; hel@whut.edu.cn; Fax: +86-27-87644867; Tel: +86-27-87467595*

[b] *Department of Mathematics and Physics, Luoyang Institute of Science and Technology, Luoyang 471023, People's Republic of China*

† Electronic supplementary information (ESI) available. See DOI: 10.1039/c6ra06864b

Supercapacitor, as an essential electric energy storage and supply device with high power density and great cycling stability, has drawn many attentions.[22–24] Substantial efforts have been made to optimize the carbon electrodes and structures of the supercapacitors to obtain high performance.[25,26] The C-MEMS is a unique and powerful platform for optimization, integration and characterization of carbon microelectrodes for applications in energy storage devices because of the fine patterning and various characteristics of carbon (*e.g.*, wide electrochemical window, chemical inertness, high thermal stability, high specific surface area, good conductivity and abundance).[27–30]

For the pyrolyzed carbon based composite, the carbon/metal oxide (electrochemically active materials, *e.g.*, NiO, MnO_2, MoO_3, WO_3, *etc.*) composite is considered as one kind of the most promising materials for supercapacitors due to its high electric conductivity, high capacitance and chemical stability.[31–37] Therefore, the microstructuring of carbon/metal oxide composite is an effective and important approach for supercapacitors to obtain high energy density and enhanced mechanical stability.[38,39]

NiO is considered as an alternative electrode material for electrochemical supercapacitor due to its facile synthesis, relatively high specific capacitance (theoretical specific capacitance of 3750 F g^{-1}), environmental friendliness and low cost. However, using NiO as the electrode material for electrochemical supercapacitor has some challenges, such as poor cycling performance and high resistivity.[40] Recently, compositing NiO with conductive metal and carbon materials is considered as an effective approach.[41–45] Transformation of metal oxide into metal through the reduction reaction is an effective method to obtain conductive metal.[37,45] Herein, the carbon/NiO/Ni (C/NiO/Ni) microelectrodes are fabricated and investigated to realize high performance integrated C-MEMS.

2. Experimental

2.1. Preparation of NiO hollow nanospheres

In our synthesis procedure, all reagents are analytical grade and used as received without further purification. The templates of carbon nanospheres were prepared according to the modified method of previous studies.[46,47] Typically, 0.8 g glucose was dissolved in 80 mL deionized water and stirred with a magnetic stirrer to get a clear solution in a beaker. Then the pH was adjusted to ~8 by adding 1 M NaOH in the solution. The solution was heated in water bath at 80 °C for 3 h. After these steps, the solution was transferred into a 100 mL Teflon-lined autoclave, heated and maintained at 180 °C for 5 h, and cooled to room temperature naturally. The brown products were washed with ethanol and deionized water for several times by centrifugation, and dried at 60 °C for 12 h.

For the preparation of $C/Ni(OH)_2$ precursor and NiO hollow nanospheres (Fig. 1), 0.072 g synthesized carbon spheres were dispersed in 40 mL 0.005 M $NiSO_4 \cdot 6H_2O$ solution by stirring for 1 h to ensure that metal ions can be sufficiently adsorbed on the surface of carbon spheres.[46] Then 0.25 g urea was added and the solution was stirred for 1 h. The brown solution was transferred into a flask and reacted at 90 °C for 8 h and the suspension was cooled to room temperature and centrifuged to obtain the $C/Ni(OH)_2$ precursors. The black products were washed by ethanol and dried at 60 °C for 12 h. Afterwards, the precursors were annealed at 450 °C for 4 h with a heating rate of 2 °C min^{-1} in air, and the NiO hollow nanospheres were obtained.

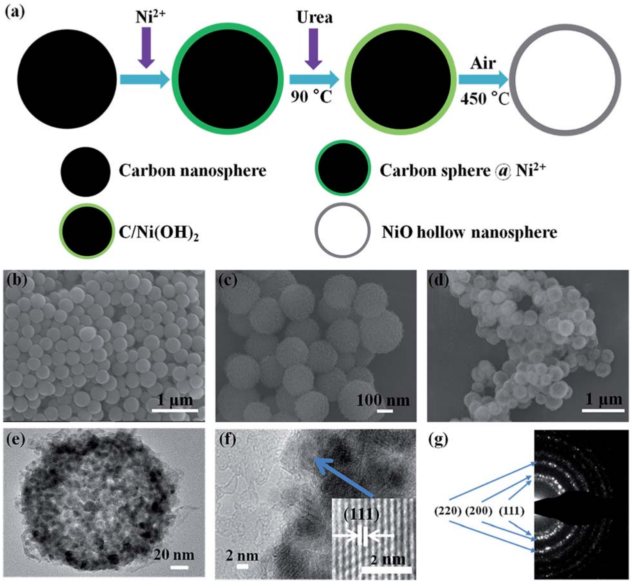

Fig. 1 (a) Schematic diagram of synthesis of NiO hollow nanospheres. (b) SEM image of carbon spheres used as templates, (c) $C/Ni(OH)_2$ precursor, and (d) NiO hollow nanospheres, respectively. (e) TEM image of NiO hollow nanosphere. (f) Magnified TEM image of NiO hollow nanospheres, inset is the HR-TEM image of the NiO hollow nanospheres. (g) Electron diffraction pattern of NiO hollow nanospheres.

2.2. Microfabrication of carbon/NiO/Ni microelectrodes based microsupercapacitor

The microfabrication process of the C/NiO/Ni microelectrodes based microsupercapacitor consists of three steps: (a) NiO hollow nanospheres were mixed with PR1-9000A photoresist (Futurrex), and a spin coating of the photoresist/NiO on the substrate; (b) patterning of the photoresist/NiO composite; (c) pyrolysis process of the micropatterned composite, as shown in Fig. 2. NiO hollow nanospheres were mixed with PR1-9000A photoresist (weight percent of NiO: 5%). The mixture was probe sonicated and stirred for 6 h to achieve a uniform photoresist/NiO composite. The composite was spin-coated on Si/SiO_2 substrate (500 nm oxide layer) by 1000 rpm for 10 s, and 4000 rpm for 40 s. Then the sample was pre-baked at 100 °C for 15 min. Followed by an optimized photolithography, development and rinse with longer time than those of standard treatment of PR1-9000A photoresist. Afterwards, the patterned interdigital microelectrodes were post-baked at 115 °C for 30 min. The sample was loaded into a hot-wall chemical vapor deposition furnace. After purging for several minutes in N_2, the furnace was heated to 400 °C for 1 h with a heating rate of 2 °C min^{-1} and held at this temperature for 1 h. The temperature

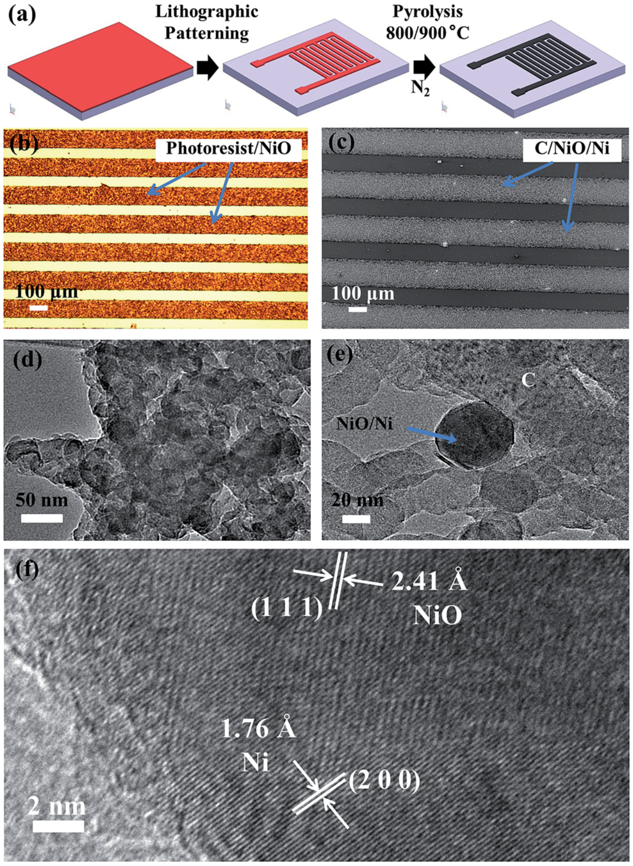

Fig. 2 (a) Schematic of fabrication process of patterned C/NiO/Ni microelectrodes. (b) Optical image of patterned photoresist/NiO composite. (c) SEM image of patterned C/NiO/Ni microelectrodes *via* pyrolysis of photoresist/NiO. (d) TEM image of patterned C/NiO/Ni microelectrodes *via* pyrolysis of photoresist/NiO. (e) Magnified TEM image of C/NiO/Ni composite. (f) HR-TEM image of C/NiO/Ni composite.

then increased at a rate of 2 °C min^{-1} to 900 °C, and the sample was annealed at 900 °C for 1 h. After the 900 °C pyrolysis, the furnace was cooled to room temperature naturally. The pyrolysis and cooling process were under N_2 atmosphere.

2.3. Characterization

X-ray diffraction (XRD) was performed using a Bruker D8 Discover X-ray diffractometer with a non-monochromated Co Kα X-ray source ($\lambda = 1.7902$ Å) at room temperature. Scanning electron microscopy (SEM) images were collected with a JEOL JSM-7100F SEM at an acceleration voltage of 15 kV. Transmission electron microscopy (TEM) and high resolution transmission electron microscopy (HR-TEM) images were recorded using a Titan G^2 60-300 Probe Cs Corrector HRSTEM. X-ray photoelectron spectroscopy (XPS) measurements were performed using a VG MultiLab 2000 instrument. Raman spectra were acquired using a Renishaw RM-1000 laser Raman microscopy. Thermogravimetry (TG) was performed using a Netzsch STA 449C simultaneous thermal analyzer at a heating rate of 10 °C min^{-1} in nitrogen. The electrochemical performances were evaluated by a commercial potentiostat (AC Instruments, 660D Model), Autolab 302N combined with probe station (Lake shore, TTPX).

3. Results and discussion

3.1. Characterization of the sample before and after pyrolysis

In this research, for integration of hydrothermally synthesized NiO hollow nanospheres with carbon-based microdevice, a microfabrication process of optimized photolithography and pyrolysis is investigated and developed. The high crystallinity NiO hollow nanospheres with a diameter of ~200 nm were synthesized by a modified method, as shown in Fig. 1a. The synthesis was performed with carbon nanospheres as templates (Fig. 1b), and C/Ni(OH)$_2$ as precursor (Fig. 1c). The synthesized NiO hollow nanospheres by 450 °C annealing in air with a uniform size are shown in Fig. 1d. For the structural characterization of as-synthesized NiO hollow nanospheres, the XRD pattern indicates the pure phase of NiO (Fig. S1†), the TEM image clearly shows the hollow structure (Fig. 1e). The high crystallinity of NiO hollow nanospheres is confirmed by the HR-TEM image with (111) lattice plane shown in Fig. 1f. The polycrystal structure of NiO hollow nanospheres can be clearly demonstrated in the electron diffraction pattern, as shown in Fig. 1g.

In our microfabrication process (Fig. 2a), the patterned photoresist/NiO composite was converted to C/NiO/Ni during the pyrolysis process under inert N_2 atmosphere. Fig. 2b shows the optical image of photoresist/NiO interdigital micropatterns (each having 7 fingers with a size of 0.28 × 0.018 cm^2). The scanning electron microscopy (SEM) image of C/NiO/Ni microelectrodes by carbonization is shown in Fig. 2c. The fine patterning of composite can be well reserved during the pyrolysis process. The thickness of C/NiO/Ni composite is ~1.5 μm after pyrolysis at 900 °C by surface profiler. Detailed morphology and structure can be identified by TEM and HR-TEM images (Fig. 2d–f). It is clear that NiO/Ni nanospheres with a diameter of ~50 nm are uniformly dispersed in carbon matrix. However, some NiO hollow nanospheres are destroyed after partly reduced to Ni. HR-TEM image (Fig. 2f) indicates clearly the Ni and NiO phases according to (200) and (111) lattice planes, respectively. The internal NiO and the outer layer of Ni are co-existed in one nanosphere. The pyrolyzed carbon is embedded with NiO/Ni nanospheres. This unique structure provides high electrical conductivity, and the embedded Ni layer can accommodate the mechanical strain since the Ni is a material with high toughness and plastic deformation.[44,45,48]

The thermogravimetric analysis (TGA) measurement of PR1-9000A photoresist was performed to determine the weight percent of pyrolyzed carbon of the composite. As shown in Fig. 3a, several regions of weight loss can be observed with temperature increasing. During the pyrolysis, 83.8% and 84.7% weight loss occurred at 800 and 900 °C, respectively. The photoresist/NiO (weight ratio of 95 : 5) was converted to C/NiO/Ni with the weight percent of carbon ranging from 74.4% to 78.3% at 900 °C according to the TGA result. Micro Raman

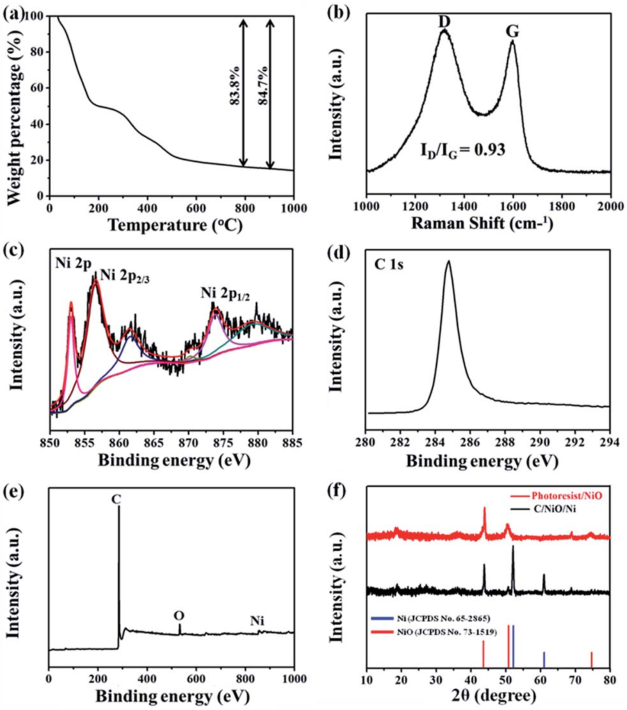

Fig. 3 (a) TGA curve of PR1-9000A photoresist. (b) Raman spectrum of C/NiO/Ni composite by 900 °C pyrolysis. (c) XPS spectrum for Ni 2p of C/NiO/Ni composite by 900 °C pyrolysis. (d) XPS spectrum for C 1s of C/NiO/Ni composite (900 °C). (e) XPS survey spectrum of C/NiO/Ni composite (900 °C). (f) XRD patterns of photoresist/NiO and C/NiO/Ni (900 °C).

spectroscopy was utilized to measure the carbonaceous peaks of C/NiO/Ni microelectrode. Two distinct carbonaceous peaks of C/NiO/Ni microelectrode in Raman spectrum (Fig. 3b) centered at ∼1350 and ∼1600 cm^{-1} are ascribed to the disorder-induced band (D-band) and the graphitic band (G-band), respectively. The D-band of the microcrystallite graphite is due to the enhanced double resonance Raman scattering, the G-band is ascribed to the bond stretching motion pairs of sp^2 C atoms present in the olefinic chains or the aromatic rings. A corresponding intensity ratio (I_D/I_G) of 0.93 is obtained indicating greater graphitization for amorphous carbon structures than those of carbon fabricated from SU-8 and AR-UL-01 precursors.[14,22] In addition, the Raman spectrum of the unpyrolyzed photoresist was not obtainable since it is strongly fluorescent.

The X-ray photoelectron spectroscopy (XPS) analysis was conducted. In Fig. 3c, three peaks for Ni $2p_{3/2}$ at 850–867 eV and three peaks for Ni $2p_{1/2}$ at 867–885 eV appear in the high-resolution XPS spectrum of Ni 2p. The strong peak at 855.6 eV for Ni $2p_{3/2}$ and 873.8 eV for Ni $2p_{1/2}$ are assigned to Ni^{2+}, while the weak satellite peaks at 852.5 and 869.8 eV are attributed to the Ni–Ni bond, respectively. The peaks at 861.5 and 880.1 eV are satellite peaks attributed to the Ni $2p_{3/2}$ and Ni $2p_{1/2}$ spin orbit levels of NiO. The XPS curve for C 1s (284.6 eV) is consistent with previous reported results (Fig. 3d).[22] XPS survey spectrum is shown in Fig. 3e. The XPS results indicated the existence of carbon, NiO and Ni in the microelectrodes. The photoresist/NiO and C/NiO/Ni composites were characterized by XRD (Fig. 3f). The characteristic peaks of NiO and Ni are observed because the photoresist/NiO composite has converted to C/NiO/Ni composite after pyrolysis. The peaks at $2\theta = \sim 18°$ and 68° appear in both patterns, which result from the substrate.[49]

3.2. Electrochemical properties of the microsupercapacitors

The electrochemical performance of the microsupercapacitor was measured *via* cyclic voltammetry (CV), galvanostatic charge/discharge, and AC impedance spectroscopy using a commercial potentiostat. All of the electrochemical measurements were performed with an aqueous electrolyte of 1 M KOH. Fig. 4a shows the current *vs.* applied voltage between the two electrodes of supercapacitor over a 0.6 V potential window at a scan rate of 10 mV s^{-1}. The specific capacitance (C) can be calculated by the following equation,[50]

$$C = \frac{I_{\text{avg}}}{sA} \tag{1}$$

where I_{avg} is the average current magnitude of the cathodic and anodic sweep, s is the voltage scan rate and A is the electrode area covered by electrolyte, measured as 0.0927 mm^2. The CV curve of C/NiO/Ni microelectrodes based supercapacitor is similar to that of supercapacitor with pyrolyzed carbon microelectrodes derived from patterned PR1-9000A. At a scan rate of 10 mV s^{-1}, the specific capacitance of C/NiO/Ni microelectrodes is 2.75 mF cm^{-2}, which is higher than that of pure pyrolyzed carbon microelectrodes (2.07 mF cm^{-2}). The CV curves of pure carbon and C/NiO/Ni composite deviate from quasi-rectangular shape indicate the occurrence of reversible surface reactions occurring at the electrodes, in the electrolyte, or both.[50,51] These

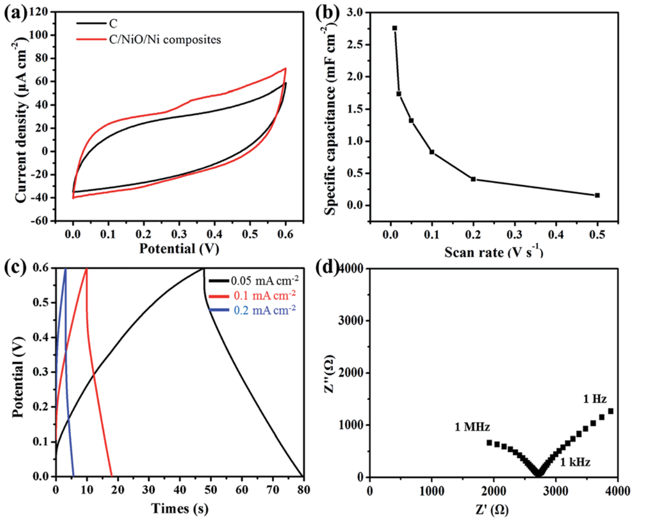

Fig. 4 (a) Cyclic voltammograms of the pure pyrolyzed carbon and C/NiO/Ni microelectrodes based supercapacitors. (b) Specific capacitance of C/NiO/Ni microelectrodes based supercapacitor at different scan rates. (c) Galvanostatic charge/discharge curves for C/NiO/Ni microelectrodes based supercapacitor at different specific currents. (d) AC impedance curves of C/NiO/Ni microelectrodes based supercapacitor.

reversible surface reactions are the result of surface oxygen-containing functional groups on the pyrolyzed carbon and electrochemically active NiO.[52] The absence of redox peaks in the CV curve indicates that C/NiO/Ni microelectrodes based supercapacitor is charged/discharged at a pseudoconstant rate over the entire voltammetric cycles. The effect of the scan rate on capacitance is clearly shown in Fig. 4b. The specific capacitance drops rapidly from 2.75 to 0.15 mF cm^{-2} with increasing scan rate from 0.01 to 500 mV s^{-1} which contribute to the insufficient time available for ion diffusion and adsorption into electrode materials at high scan rate.[21] Galvanostatic charge/discharge processes of the fabricated device were performed at three representative specific currents and the curves are presented in Fig. 4c. Pseudolinear discharge curves are observed for all applied currents. The charge and discharge curves with non-linearity prove that the contribution of faradic reactions to the capacitance, since an ideally polarisable electrode with no charge transfer to the electrolyte has linear charge and discharge behaviours. The equivalent series resistance (ESR) of device can be estimated to be ~1000 Ω cm^{-2} at various current densities using the magnitude of the IR drops. Such large value of ESR may be attributed to the sharp decrease in capacitance with increasing scan rate as shown in Fig. 4b.[50] The AC impedance spectroscopy curve of the microsupercapacitor is shown in Fig. 4d. The ESR value of ~1000 Ω cm^{-2} can be fitted from the *x*-intercept of the Nyquist plot shown in Fig. 4d, which is in reasonable agreement with the estimation from galvanostatic charge/discharge measurements.

For energy storage devices in practical applications, high energy and power densities are required. The theoretical energy and power densities of the supercapacitor can be calculated according to eqn (2):[21,45]

$$E = \frac{1}{2}CV^2 \tag{2}$$

where C is the specific capacitance, V is the maximum voltage window and Δt is the discharge time. At a voltage window of 0 to 0.6 V, the theoretical energy density of 0.92 mW h cm^{-3} is obtained.

A long-term cycling test was performed *via* repetitive CV scans at a scan rate of 1 V s^{-1} (Fig. 5). The retained capacitance percent as a function of the cycle number is obtained, and the capacitance of micro-supercapacitor retains ~95% after 1000 cycles. The high specific capacitance and less degradation during the cycling test result from the unique porous structure of C/NiO/Ni composite, which enables easy access of OH$^-$ into the composite microelectrode.

The formation of NiO/Ni nanospheres and carbon macropores can be described as the process shown in Fig. S2.† The uniformly dispersed NiO hollow nanospheres deformed and collapsed in the matrix gradually during the pre-carbonization stage, also some smaller NiO nanospheres formed and agglomerated together. NiO nanospheres that contact with carbon were reduced to Ni, and some macropores (Fig. S3†) in the carbon were formed since the reduction consumed small amount of carbon. Finally, NiO/Ni and Ni nanospheres were obtained and embedded in carbon matrix. In addition, the mechanical properties of Ni and NiO are better than that of pyrolyzed carbon, such as higher Young's modulus, higher toughness, higher ductibility, *etc.* Therefore, the enhanced capacitance of C/NiO/Ni microelectrodes based supercapacitor with higher mechanical stability compared with that of pure pyrolyzed carbon based supercapacitor should result from the capacitance of residual NiO, although some carbon and NiO have been consumed during the pyrolysis process. Also, the macropores of carbon make the electrolyte easily access the C/NiO/Ni microelectrodes, and more ions can be transported in the electrochemical process.

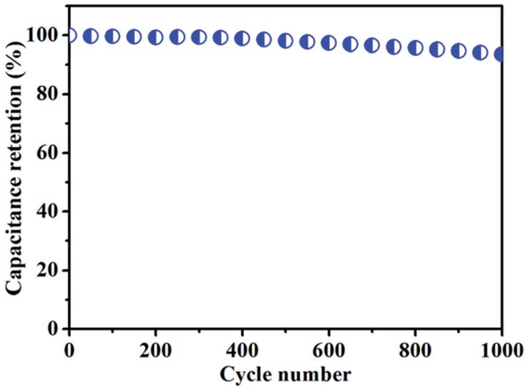

Fig. 5 Cycling performance of the carbon/NiO/Ni microelectrodes based microsupercapacitor.

4. Conclusions

The C/NiO/Ni microelectrodes based supercapacitor by optimized C-MEMS fabrication is achieved and investigated. The fabricated C/NiO/Ni microelectrodes reinforced by uniformly dispersed NiO/Ni nanospheres show improved capacitance compared with that of the pure pyrolyzed carbon microelectrodes. The fine patterned C/NiO/Ni microelectrode served both as current collector and electrochemical active material for the supercapacitors, which demonstrates the facility and compatibility of this fabrication process. This optimized fabrication and integration approach has great potential for carbon based composite and applications in microdevices and microsystem.

Acknowledgements

This work was supported by the National Basic Research Program of China (2013CB934103 and 2012CB933003), the National Natural Science Fund for Distinguished Young Scholars (51425204), the National Natural Science Foundation of China (51521001 and 51502227), the China Postdoctoral Science Foundation (2015T80845), and the Fundamental Research Funds for the Central Universities (WUT: 2014-IV-062, 2014-IV-147, 2014-YB-002, and 2016III005).

Notes and references

1 L. He, M. Toda, Y. Kawai, M. F. SarbiM, M. Omori, T. Hashida and T. Ono, *IEEJ Trans. Sens. Micromach.*, 2012, **132**, 425–426.

2 L. He, M. Toda, Y. Kawai, H. Miyashita, M. Omori, T. Hashida, R. Berger and T. Ono, *Microsyst. Technol.*, 2014, **20**, 201–208.

3 P. Zhou, X. Yang, L. He, Z. M. Hao, W. Luo, B. Xiong, X. Xu, C. J. Niu, M. Y. Yan and L. Q. Mai, *Appl. Phys. Lett.*, 2015, **106**, 111908.

4 Z. Y. Cai, L. Xu, M. Y. Yan, C. H. Han, L. He, K. M. Hercule, C. J. Niu, Z. F. Yuan, W. W. Xu, L. B. Qu, K. N. Zhao and L. Q. Mai, *Nano Lett.*, 2015, **15**, 738–744.

5 X. C. Tian, M. Z. Shi, X. Xu, M. Y. Yan, L. Xu, A. Minhas-Khan, C. H. Han, L. He and L. Q. Mai, *Adv. Mater.*, 2015, **27**, 7476–7482.

6 M. F. L. De Volder, R. Vansweevelt, P. Wagner, D. Reynaerts, C. V. Hoof and A. J. Hart, *ACS Nano*, 2011, **5**, 6593–6600.

7 L. Wei, N. Nitta and G. Yushin, *ACS Nano*, 2013, **7**, 6498–6506.

8 W. Chen, M. Beidaghi, V. Penmatsa, K. Bechtold, L. Kumari, W. Z. Li and C. L. Wang, *IEEE Trans. Nanotechnol.*, 2010, **9**, 734–740.

9 M. Hirabayashi, B. Mehta, B. Nguyen and S. Kassegne, *Microsyst. Technol.*, 2015, **21**, 2359–2365.

10 S. Kassegne, M. Vomero, R. Gavuglio, M. Hirabayashi, E. Özyilmaz, S. Nguyen, J. Rodriguez, E. Özyilmaz, P. V. Niekerk and A. Khosla, *Microelectron. Eng.*, 2015, **133**, 36–44.

11 S. W. Li and X. H. Wang, *J. Power Sources*, 2015, **282**, 394–400.

12 L. Amato, A. Heiskanen, R. Hansen, L. Gammelgaard, T. Rindzevicius, M. Tenje, J. Emnéus and S. S. Keller, *Carbon*, 2015, **94**, 792–803.

13 S. L. Jiang, T. L. Shi, D. Liu, H. Long, S. Xi, F. S. Wu, X. P. Li, Q. Xia and Z. R. Tang, *J. Power Sources*, 2014, **262**, 494–500.

14 S. L. Jiang, T. L. Shi, Y. Gao, H. Long, S. Xi and Z. R. Tang, *J. Micromech. Microeng.*, 2014, **24**, 045001.

15 M. Roussel, C. Malhaire, A. L. Deman, J. F. Chateaux, L. Petit, L. Seveyrat, J. Galineau, B. Guiffard, C. Seguineau, J. M. Desmarres and J. Martegoutte, *J. Micromech. Microeng.*, 2014, **24**, 055011.

16 G. Canton, T. Do, L. Kulinsky and M. Madou, *Carbon*, 2014, **71**, 338–342.

17 S. Xi, T. L. Shi, D. Liu, L. L. Xu, H. Long, W. X. Lai and Z. R. Tang, *Sens. Actuators, A*, 2013, **198**, 15–20.

18 S. W. Lee, C. H. Lee, J. A. Lee and S. S. Lee, *Nanotechnology*, 2013, **24**, 025301.

19 H. Mekaru, C. Okuyama and A. Ueno, *Microsyst. Technol.*, 2013, **19**, 315–323.

20 C. W. Shen, X. H. Wang, S. W. Li, J. G. Wang, W. F. Zhang and F. Y. Kang, *J. Power Sources*, 2013, **234**, 302–309.

21 B. Hsia, M. S. Kim, M. Vincent, C. Carraro and R. Maboudian, *Carbon*, 2013, **57**, 395–400.

22 V. Penmatsa, H. Kawarada and C. L. Wang, *J. Micromech. Microeng.*, 2012, **22**, 045024.

23 L. Zhang, T. L. Shi, Z. R. Tang, D. Liu and S. Xi, *J. Microelectromech. Syst.*, 2012, **21**, 1445–1451.

24 S. Sharma, A. Sharma, Y. K. Cho and M. Madou, *ACS Appl. Mater. Interfaces*, 2012, **4**, 34–39.

25 D. Liu, T. L. Shi, Z. R. Tang, L. Zhang, S. Xi, X. P. Li and W. X. Lai, *Nanotechnology*, 2011, **22**, 465601.

26 S. W. Lee, B. M. Gallant, H. R. Byon, P. T. Hammond and Y. Shao-Horn, *Energy Environ. Sci.*, 2011, **4**, 1972–1985.

27 D. Jariwala, V. K. Sangwan, L. J. Lauhon, T. J. Marks and M. C. Hersam, *Chem. Soc. Rev.*, 2013, **42**, 2824–2860.

28 M. Beidaghi, W. Chen and C. L. Wang, *J. Power Sources*, 2011, **196**, 2403–2409.

29 F. Galobardes, C. Wang and M. Madou, *Diamond Relat. Mater.*, 2006, **15**, 1930–1934.

30 R. L. McCreery, *Chem. Rev.*, 2008, **108**, 2646–2687.

31 J. Jang, J. Bae, M. Choi and S. H. Yoon, *Carbon*, 2005, **43**, 2730–2736.

32 L. Wei and G. Yushin, *Nano Energy*, 2012, **1**, 552–565.

33 L. Wei, M. Sevilla, A. B. Fuertes, R. Mokaya and G. Yushin, *Adv. Funct. Mater.*, 2012, **22**, 827–834.

34 J. Tang, J. Liu, N. L. Torad, T. Kimura and Y. Yamauchi, *Nano Today*, 2014, **9**, 305–323.

35 M. P. Yeager, D. Su, N. S. Marinković and X. W. Teng, *J. Electrochem. Soc.*, 2012, **159**, A1598–A1603.

36 M. J. Zhi, C. C. Xiang, J. T. Li, M. Li and N. Q. Wu, *Nanoscale*, 2013, **5**, 72–88.

37 R. J. Huo, W. J. Jiang, S. L. Xu, F. Z. Zhang and J. S. Hu, *Nanoscale*, 2014, **6**, 203–206.

38 R. B. Du, S. Ssenyange, M. Aktary and M. T. McDermott, *Small*, 2009, **5**, 1162–1168.

39 M. Sevilla and R. Mokaya, *Energy Environ. Sci.*, 2014, **7**, 1250–1280.

40 G. P. Wang, L. Zhang and J. J. Zhang, *Chem. Soc. Rev.*, 2012, **41**, 797–828.

41 S. Vijayakumar, S. Nagamuthu and G. Muralidharan, *ACS Sustainable Chem. Eng.*, 2013, **1**, 1110–1118.

42 C. H. Wu, S. X. Deng, H. Wang, Y. X. Sun, J. B. Liu and H. Yan, *ACS Appl. Mater. Interfaces*, 2014, **6**, 1106–1112.

43 Y. Bai, M. Du, J. Chang, J. Sun and L. Gao, *J. Mater. Chem. A*, 2014, **2**, 3824–3840.

44 F. Zou, Y. M. Chen, K. W. Liu, Z. T. Yu, W. F. Liang, S. M. Bhaway and M. Gao, *ACS Nano*, 2016, **10**, 377–386.

45 Z. Q. Liang, R. J. Huo, Y. X. Yin, F. Z. Zhang, S. L. Xu and Y. G. Guo, *Electrochim. Acta*, 2013, **108**, 429–434.

46 Z. H. Yang, F. F. Xu, W. X. Zhang, Z. S. Mei, B. Pei and X. Zhu, *J. Power Sources*, 2014, **246**, 24–31.

47 L. Shen, L. Yu, X. Y. Yu and X. W. Lou, *Angew. Chem., Int. Ed.*, 2015, **54**, 1868–1872.

48 Z. L. An, L. He, M. Toda, G. Yamamoto, T. Hashida and T. Ono, *Nanotechnology*, 2015, **26**, 195601.

49 L. He, Z. C. Li and Z. J. Zhang, *Nanotechnology*, 2008, **19**, 155606.

50 S. Wang, B. Hsia, C. Carraro and R. Maboudian, *J. Mater. Chem. A*, 2014, **2**, 7997–8002.

51 B. E. Conway, V. Birss and J. Wojtowicz, *J. Power Sources*, 1997, **66**, 1–14.

52 B. Hsia, M. S. Kim, C. Carraro and R. Maboudian, *J. Mater. Chem. A*, 2013, **1**, 10518–10523.